

See discussions, stats, and author profiles for this publication at: <https://www.researchgate.net/publication/284718087>

# Chiral Platinum(II) Complexes Featuring Phosphine and Chloroquine Ligands as Cytotoxic and Monofunctional DNA-Binding Agents

ARTICLE in INORGANIC CHEMISTRY · NOVEMBER 2015

Impact Factor: 4.76 · DOI: 10.1021/acs.inorgchem.5b01647

---

READS

48

## 11 AUTHORS, INCLUDING:



Javier Ellena

University of São Paulo

410 PUBLICATIONS 2,667 CITATIONS

[SEE PROFILE](#)



Marcia Regina Cominetti

Universidade Federal de São Carlos

46 PUBLICATIONS 371 CITATIONS

[SEE PROFILE](#)



Maribel Navarro

National Institute of Metrology, Quality and ...

57 PUBLICATIONS 1,210 CITATIONS

[SEE PROFILE](#)



Alzir Batista

Universidade Federal de São Carlos

170 PUBLICATIONS 2,066 CITATIONS

[SEE PROFILE](#)

# Chiral Platinum(II) Complexes Featuring Phosphine and Chloroquine Ligands as Cytotoxic and Monofunctional DNA-Binding Agents

Wilmer Villarreal,<sup>\*,†</sup> Legna Colina-Vegas,<sup>†</sup> Clayton Rodrigues de Oliveira,<sup>†</sup> Juan C. Tenorio,<sup>‡</sup> Javier Ellena,<sup>‡</sup> Fábio C. Gozzo,<sup>§</sup> Marcia Regina Cominetti,<sup>||</sup> Antonio G. Ferreira,<sup>†</sup> Marco Antonio Barbosa Ferreira,<sup>†</sup> Maribel Navarro,<sup>▽</sup> and Alzir A. Batista<sup>\*,†</sup>

<sup>†</sup>Departamento de Química, Universidade Federal de São Carlos—UFSCar, CEP 13565-905, São Carlos-SP, Brazil

<sup>‡</sup>Instituto de Física de São Carlos, Universidade de São Paulo, CEP 13560-970, São Carlos-SP, Brazil

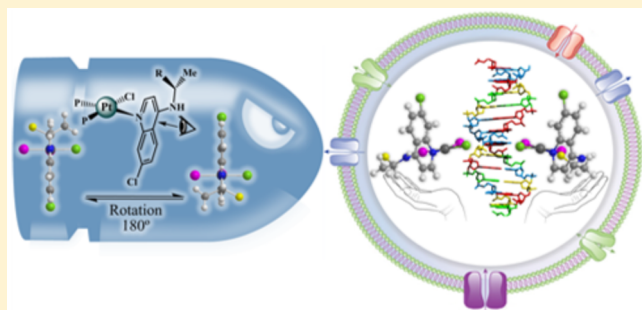
<sup>§</sup>Instituto de Química, Universidade Estadual de Campinas—UNICAMP, CEP 13083-970, Campinas-SP, Brazil

<sup>||</sup>Departamento de Gerontologia, Universidade Federal de São Carlos—UFSCar, CEP, 13565-905, São Carlos-SP, Brazil

<sup>▽</sup>Instituto Nacional de Metrologia, Qualidade e Tecnologia, INMETRO, CEP, 25250-020 Rio de Janeiro-RJ, Brazil

## Supporting Information

**ABSTRACT:** Chiral molecules in nature are involved in many biological events; their selectivity and specificity make them of great interest for understanding the behavior of bioactive molecules, by providing information about the chiral discrimination. Inspired by these conformational properties, we present the design and synthesis of novel chiral platinum(II) complexes featuring phosphine and chloroquine ligands with the general formula  $[\text{PtCl}(\text{P})_2(\text{CQ})]\text{PF}_6$  (where  $(\text{P})_2$  = triphenylphosphine ( $\text{PPh}_3$ ) (5), 1,3-bis(diphenylphosphine)propane (dppp) (6), 1,4-bis(diphenylphosphine)butane (dpbb) (7), 1,1'-bis(diphenylphosphine)ferrocene (dpfp) (8), and CQ = chloroquine] and their precursors of the type  $[\text{PtCl}_2(\text{P})_2]$  are described. The complexes were characterized by elemental analysis, absorption spectroscopy in the infrared and ultraviolet-visible (UV-vis) regions, multinuclear ( $^1\text{H}$ ,  $^{13}\text{C}$ ,  $^{31}\text{P}$ ,  $^{15}\text{N}$ , and  $^{195}\text{Pt}$ ) NMR spectroscopy, cyclic voltammetry, and mass spectrometry (in the case of chloroquine complexes). The interactions of the new platinum–chloroquine complexes with both albumin (BSA), using fluorescence spectroscopy, and DNA, by four widely reported methods were also evaluated. These experiments showed that these Pt-CQ complexes interact strongly with DNA and have high affinities for BSA, in contrast to CQ and CQDP (chloroquine diphosphate), which interact weakly with these biomolecules. Additional assays were performed in order to investigate the cytotoxicity of the platinum complexes against two healthy cell lines (mouse fibroblasts (L929) and the Chinese hamster lung (V79-4)) and four tumor cell lines (human breast (MDA-MB-231 and MCF-7), human lung (A549), and human prostate (DU-145)). The results suggest that the Pt-CQ complexes are generally more cytotoxic than the free CQ, showing that they are promising as anticancer drugs.



## INTRODUCTION

Since Rosenberg's serendipitous discovery<sup>1</sup> opened the pathway for the introduction of metal complexes in antineoplastic chemotherapy, several platinum(II) complexes (i.e., cisplatin, carboplatin, and oxaliplatin) have become mainstays in cancer treatment.<sup>2</sup> However, the cross resistance and severe side effects of platinum drugs have limited their clinical application, to a great extent. In order to overcome these drawbacks, many drug design strategies have been used,<sup>3</sup> and over the last 25 years, one attractive procedure—the so-called “metal–drug synergism”—can be achieved by combining an organic compound with a known activity and a metal-based complex, searching for synergistic action against several pathogens, including tumor cells.<sup>4</sup> Thus, several researchers have focused on elucidating the mechanism of action of these complexes, to

guide the rational synthesis of new platinum drugs and/or improve the activity of known platinum-based drugs used in chemotherapy.<sup>5</sup>

One of life's distinctive biochemical signatures is the high selectivity of chiral molecular species, and the use of chiral metal complexes to probe the structure of DNA and other biomolecules is an active area of research at the interface of chemistry and biology.<sup>6</sup> As a result, many biological events are greatly influenced by the chirality of molecules.<sup>7</sup> The process by which chiral reagents are able to recognize different local structures along the DNA strand is governed by systems in which the asymmetry and size of the complex are the most

Received: July 27, 2015

important aspects. Thus, chiral metal complexes provide very sensitive probes for the local helical structure of the DNA, both left-handed and right-handed.<sup>8</sup> A previous study investigating the interaction between chiral metal complexes and biomolecules, particularly with inherently chiral DNA and protein, furnished information about the chiral discrimination of diastereomers, helping in the discovery of important leads for developing targeted bioactive molecules.<sup>9</sup>

Lippard et al. started the applications of chiral platinum complexes as anticancer agents in the early 1990s, substituting one chlorido of the cisplatin for one molecule of chloroquine.<sup>10</sup> Recently, a systematic variation of the N-heterocyclic ligands in compounds of the formula *cis*-[Pt(NH<sub>3</sub>)<sub>2</sub>(Am)Cl]<sup>+</sup> (where Am denotes a N-heterocyclic ligand), resulting in the monofunctional DNA-binding phenanthriplatin, which showed greater efficacy than cisplatin and oxaliplatin in established human cancer cells, has revealed a distinct pattern of activity.<sup>11</sup> This year, it was found that the activity of the phenanthriplatin complex was related to its chirality and its interconversion phenomenon.<sup>12</sup>

In this work, we combine the DNA covalent binding characteristics of platinum complexes<sup>13</sup> with the chemical properties of phosphines,<sup>14</sup> together with chloroquine, which is the most successful drug used to treat malaria, it also has several biological effects, such as inhibition of cell growth and/or induction of death in different types of cells,<sup>15–18</sup> to obtain four chiral Pt(II)/phosphine–chloroquine complexes (MDA-MB-231, MCF-7, A549, and DU-145) and healthy cell lines (L929 and V79-4), in order to evaluate their cytotoxicity against tumor cell lines. This study also describes investigations into the interaction of the *cis*-[PtCl(CQ)(PPh<sub>3</sub>)<sub>2</sub>]PF<sub>6</sub> (**5**), [PtCl(CQ)(dppp)]PF<sub>6</sub> (**6**), [PtCl(CQ)(dppb)]PF<sub>6</sub> (**7**), and [PtCl(CQ)(dppf)]PF<sub>6</sub> (**8**) compounds (where PPh<sub>3</sub> = triphenylphosphine, dppp = 1,3-bis(diphenylphosphine)propane, dppb = 1,4-bis(diphenylphosphine)butane, dppf = 1,1'-bis(diphenylphosphine)ferrocene, and CQ = chloroquine) with DNA and BSA.

## RESULTS AND DISCUSSION

**Pt-P<sub>2</sub>-CQ Complexes.** The new phosphine–chloroquine/platinum complexes **5–8** (Figure 1) were synthesized by the

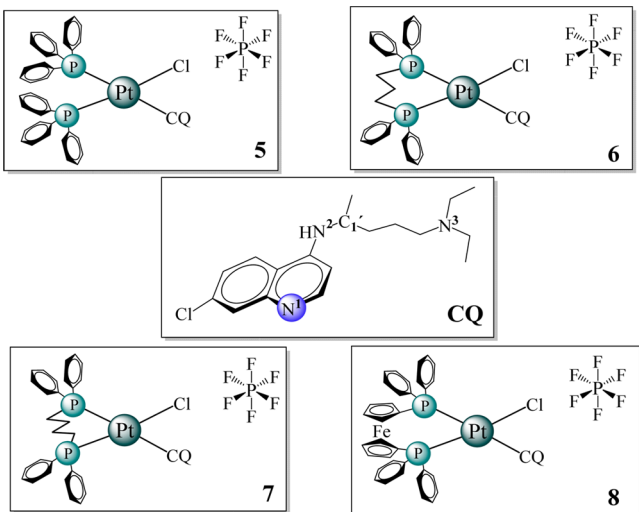


**Figure 1.** Structures suggested for the new Pt(II)/phosphine–chloroquine complexes.

substitution of a chlorido ligand by one CQ molecule in the precursors **1–4** with the general formula [PtCl<sub>2</sub>(P)<sub>2</sub>] (where (P)<sub>2</sub> denotes PPh<sub>3</sub> (**1**), dppp (**2**), dppb (**3**), or dppf (**4**)), employing PF<sub>6</sub><sup>−</sup> as the anion to stabilize the cationic species. Thus, complexes **5–8** were isolated in good yields, as white or yellow solids (see the [Experimental Section in the Supporting Information](#)). The elemental analyses of these complexes were in agreement with the proposed molecular formula. The UV-vis spectra of the complexes displayed bands associated with the presence of coordinated CQ, at 348 and 358 nm, corresponding to π–π\* transitions from the quinoline rings, and at 235 nm corresponding to π–π\* transitions from the phosphine ligands. In the IR spectra of the complexes, the characteristic bands of chloroquine were observed, such as a strong absorption band at 3410 cm<sup>−1</sup>, assigned to NH stretching vibrations. This band showed a difference of 180 cm<sup>−1</sup>, when compared with the free CQ ligand. The band corresponding to C=N vibrations in the complexes was observed at 1548 cm<sup>−1</sup>, whereas, in the free ligand, it was at 1573 cm<sup>−1</sup>. The far-infrared (FIR) spectra of the complexes showed a band at 310 cm<sup>−1</sup> assigned to Pt–Cl vibrations for complexes **5–8**, in contrast with complexes **1–4**, which presented two bands characteristic of Pt–Cl vibrations in *cis* geometry. Also, the IR of the complexes presented a band at ~520 cm<sup>−1</sup>, corresponding to ν(Pt–P), probably overlapping with ν(Pt–N).

All NMR signals of the complexes could be unequivocally assigned on the basis of one-dimensional (1D) and two-dimensional (2D) correlation spectroscopy (COSY), heteronuclear single quantum coherence (HSQC), and heteronuclear multiple bond coherence (HMBC) experiments for the complexes (for complete NMR data, see the [Experimental Section in the Supporting Information](#)). In the <sup>1</sup>H, <sup>13</sup>C{<sup>1</sup>H} and <sup>31</sup>P{<sup>1</sup>H} NMR experiments, the duplication of all signals present in the Pt(II)/phosphine–chloroquine complexes was observed. Duplication was not found in the <sup>15</sup>N and <sup>195</sup>Pt NMR experiments. This duplication indicates that the complexes displayed an axial chirality, generated by the rotation of the Pt–N<sub>1</sub> bond (atropisomerism) which, combined with the chirality of the C1' carbon in the chloroquine ligand, produced a pair of diastereomers (Figure 2). This rotation did not affect the

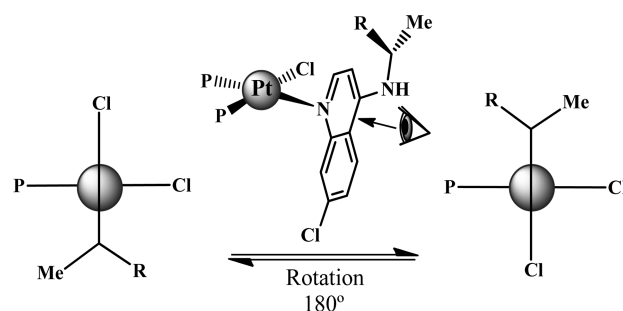


**Figure 2.** Diastereomers resulting from bond rotation of CQ around the metal center (atropisomerism).

platinum and nitrogen nuclei. This behavior has been reported for other phosphine platinum complexes with an unsymmetrical ligand, where the asymmetric center is positioned in the phosphine ligand,<sup>19</sup> as well as for other quinoline platinum(II) complexes.<sup>10,12,20</sup> The observation of both diastereomers indicates that rotation around the Pt–N<sub>1</sub> bond

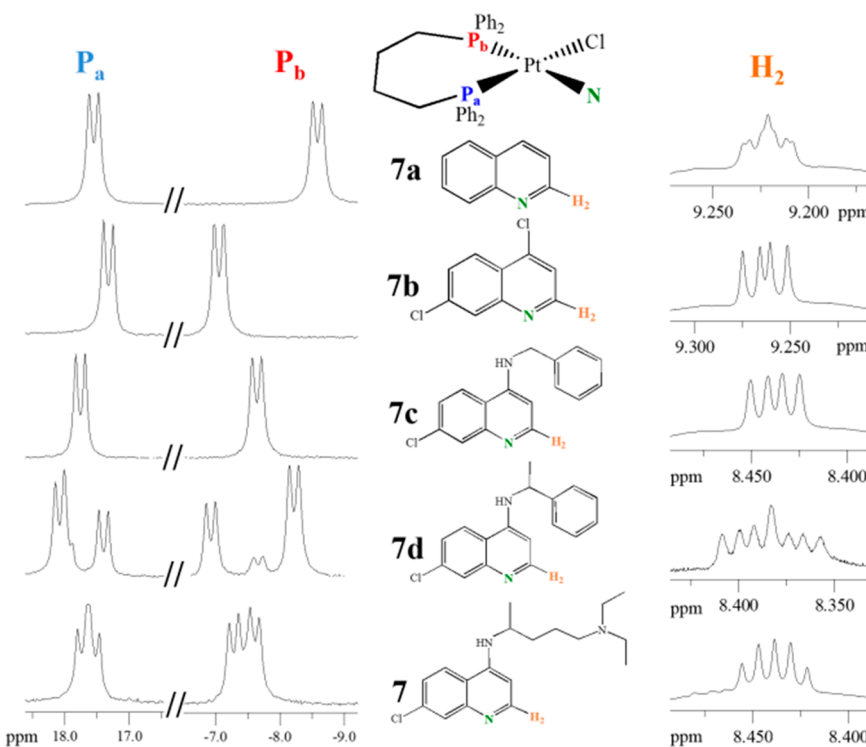


**Figure 3.**  $^{31}\text{P}\{\text{H}\}$  and  $^1\text{H}$  ( $\text{H}_2$  region) NMR spectra for modifications of complex 7 with various quinolinic ligands ((7a) quinoline, (7b) 4,7-dichloroquinoline, (7c) N-benzyl-7-chloroquinolin-4-amine, and (7d) 7-chloro- $N$ -(1-phenylethyl)quinolin-4-amine)) at 25 °C in acetone- $d_6$ .

is slow on the NMR time scale, since fast rotation would average out the effective chirality of the platinum center.<sup>10</sup>

The presence of an additional asymmetric center at the rotation of the Pt–N bond is necessary for the duplication of the signals observed in the  $^{13}\text{C}\{\text{H}\}$  and  $^{31}\text{P}\{\text{H}\}$  NMR spectra at room temperature. Thus, in order to verify the observations, a modified quinoline was used as the ligand. Also, it was also possible to show that the quinolinic ligand presented continuous twists that were only differentiated in some of its hydrogens ( $\text{H}_2$  and  $\text{H}_3$ ), since these protons are close to the center of chirality (Figure 3).<sup>21</sup> Similar behavior has been reported for other phosphine platinum and palladium complexes with an unsymmetrical ligand, where the duplication of only some hydrogens in the molecule is observed.<sup>22–24</sup>

The behavior observed in solution was also demonstrated in the solid state by X-ray experiments for the  $[\text{PtCl}(\text{dpbb})\text{-}(\text{quinoline})]\text{PF}_6$  complex (7a) (see Figure 4), which was crystallized in the centrosymmetric space group  $P2_1/c$  (see Table S1 in the Supporting Information), showing two mirror images in the same unit cell, as already reported for other quinoline platinum(II) complexes.<sup>11,12</sup> Both structures showed halogen- $\cdots\pi$  and  $\pi\cdots\pi$  interactions, allowing stabilization of the crystal packing.<sup>25</sup> The structural conformation of complex 7a shows a perpendicular orientation ( $\sim 82.52^\circ$ ) between the platinum coordination plane and the ligand quinoline plane; similarly, the phenyl group of the quinoline ligand is *syn*-oriented with the (C111–C116) and (C221–C226) phenyl rings and antioriented with the butane fragment of the dpbb ligand, with respect to the platinum coordination plane, respectively. Also, a  $\pi\cdots\pi$  intermolecular interaction was observed between the heterocyclic ring of the quinoline ligand and the (C121–C126) phenyl ring of dpbb, stabilizing the complex molecular structure. Low-temperature measurements

were carried out and no significant differences were observed in the crystalline structure of complex 7a.

The  $^1\text{H}$ ,  $^{13}\text{C}\{\text{H}\}$ , and  $^{15}\text{N}\{\text{H}\}$  chemical shift variations of each signal of the complexes, with respect to those of the free ligand (see Table S3 in the Supporting Information) were used as parameters to deduce the mode of bonding of CQ to the metal. It was previously shown by others that the largest variations for the chemical shifts of the coordinated CQ ligand, when compared with the free ligand, were always observed for the protons and carbons located in the vicinity of the N atom attached to the metal.<sup>10,26</sup> For complexes 5–8, the greatest chemical shifts, with respect to the free CQ ligand, were observed for NH, H8, H2, and H3 in the  $^1\text{H}$  NMR spectra, and C9, C8, C7, C5, and C4 in the  $^{13}\text{C}\{\text{H}\}$  NMR spectra. All other chloroquine protons and carbons showed smaller displacements, although NH had the highest variation. The other signals reveal that the chemical shifts in the quinoline region suffered from greater disturbances after ligand coordination to the metal center, indicating that CQ binds to the platinum center through the quinolinic nitrogen. This is supported by  $^{15}\text{N}\{\text{H}\}$  NMR experiments, where N<sub>1</sub> had the greatest displacement difference when compared with the free ligand (see Table 1). In the  $^{31}\text{P}\{\text{H}\}$  NMR spectra of complexes 5–8, two doublets (duplicated by the presence of the diastereomers) were observed, indicating the presence of two magnetically different P atoms coordinated to the platinum metal center. One of the P atoms was in the *trans* position, with respect to the Cl atom (P<sub>a</sub>), and the other (P<sub>b</sub>) was more shielded, in the *trans* position to the N atom of the chloroquine. All signals were flanked by satellite peaks of the respective multiplicity with an intensity of  $\sim 1:4:1$  generated for the coupling of the P atoms with the isotope  $^{195}\text{Pt}$ , the intensity is sometimes modified as a consequence of the chemical shift anisotropy relaxation of  $^{195}\text{Pt}$  nucleus.<sup>27</sup> In the  $^{195}\text{Pt}$  NMR of complexes

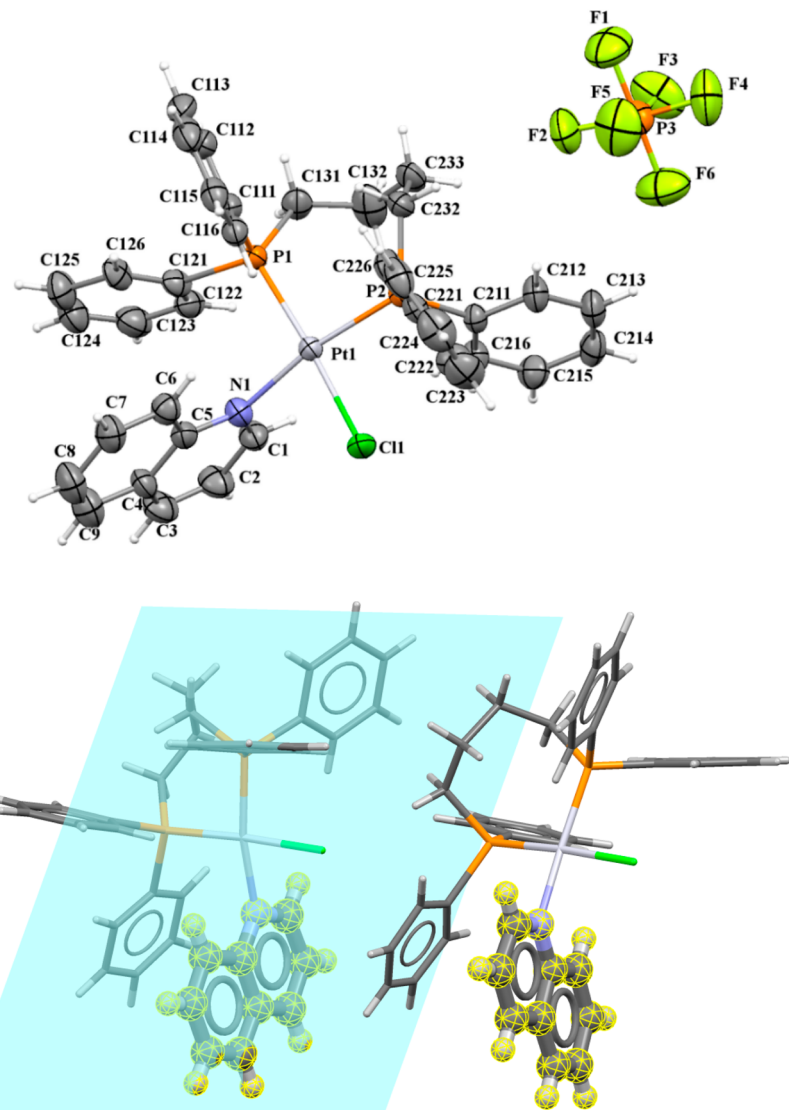


**Figure 4.** ORTEP view of the  $[\text{PtCl}(\text{dppb})(\text{quinoline})]\text{PF}_6$  complex, showing the atom labels and the 50% of probability ellipsoids (upper panel). Crystal structure of **7a** emphasizing the orientation of the quinoline ligand (lower panel).

**Table 1.**  $^{31}\text{P}\{^1\text{H}\}$ ,  $^{195}\text{Pt}\{^1\text{H}\}$ , and  $^{15}\text{N}\{^1\text{H}\}$  NMR Data for the Phosphine Pt(II) Complexes (1–8)

|  | 1                  | 2                  | 3                  | 4                  |
|--|--------------------|--------------------|--------------------|--------------------|
| $\delta$ ( $^{31}\text{P}$ ) <sup>a</sup>                    | 13.72              | −7.61              | 7.69               | 12.65              |
| $J^1$ (P–Pt) <sup>b</sup>                                    | 3681.55            | 3418.50            | 3550.51            | 3780.36            |
| $\delta$ ( $^{195}\text{Pt}$ ) <sup>a</sup>                  | −4414.02           | N/D <sup>c</sup>   | N/D <sup>c</sup>   | −4363.41           |
| $J^1$ (Pt–P) <sup>b</sup>                                    | 3670.24            | N/D <sup>c</sup>   | N/D <sup>c</sup>   | 3772.92            |
|  | 5                  | 6                  | 7                  | 8                  |
| $\delta$ ( $^{31}\text{P}_a$ ) <sup>a</sup>                  | 15.03              | −5.53              | 18.88; 19.02       | 15.26; 15.28       |
| $\delta$ ( $^{31}\text{P}_b$ ) <sup>a</sup>                  | 4.65               | −14.56; −14.46     | −9.20; −9.50       | 4.92               |
| $J^1$ (P <sub>a</sub> –Pt) <sup>b</sup>                      | 3792.85            | 3342.59            | 3589.83            | 3757.99            |
| $J^1$ (P <sub>b</sub> –Pt) <sup>b</sup>                      | 3196.44            | 2971.06            | 3002.29            | 3310.21            |
| $J^2$ (P–P) <sup>b</sup>                                     | 18.47              | 28.10              | 23.11; 22.68       | 15.42              |
| $\delta$ ( $^{195}\text{Pt}$ ) <sup>a</sup>                  | −4320.66; −4283.25 | −4399.40; −4363.23 | −4384.07; −4348.73 | −4255.16; −4216.27 |
| $J^1$ (Pt–P <sub>a</sub> ) <sup>b</sup>                      | 3707.86            | 3351.82            | 3644.15            | 3776.26            |
| $J^1$ (Pt–P <sub>b</sub> ) <sup>b</sup>                      | 3204.17            | 3012.65            | 3026.69            | 3330.5             |
| $\delta$ ( $^{15}\text{N}$ [N <sub>1</sub> ]) <sup>a,d</sup> | 350.44 (8.21)      | 350.46 (8.19)      | 350.84 (7.81)      | 350.11 (8.54)      |
| $\delta$ ( $^{15}\text{N}$ [N <sub>2</sub> ]) <sup>a,d</sup> | 342.07 (1.47)      | 342.20 (1.60)      | 342.27 (1.67)      | 342.20 (1.60)      |
| $\delta$ ( $^{15}\text{N}$ [N <sub>3</sub> ]) <sup>a,d</sup> | 336.18 (0.19)      | 336.07 (0.08)      | 336.18 (0.19)      | 336.14 (0.15)      |

<sup>a</sup>Chemical shifts (in ppm). <sup>b</sup>Coupling constant (in Hertz). <sup>c</sup>Not determined due to low solubility. <sup>d</sup>Values in parentheses correspond to the difference when compared to the free ligand.

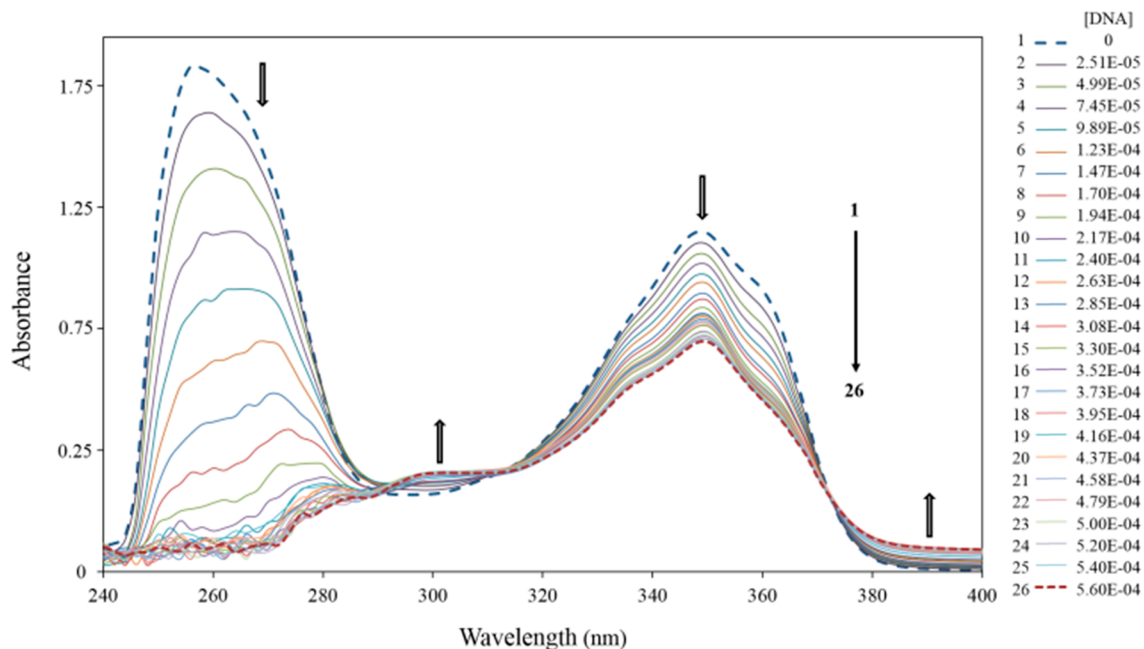


**Figure 5.** Spectrophotometric titration spectra of  $[\text{Pt}(\text{dppp})\text{CQCl}] \text{PF}_6$  with calf thymus (CT) DNA.  $[\text{Complex}] = 7.01 \times 10^{-5}$  M,  $[\text{DNA}] = 0\text{--}5.60 \times 10^{-4}$  M.

**5–8**, two doublets were observed, corresponding to the coupling of the platinum metal center, with the two magnetically different P atoms bonded to it. In the case of complexes **1–4**, a triplet was observed, generated by the coupling of the two P atoms with the same chemical environment and the platinum center.

The analysis of the NMR experiments for the atoms involved in the coordination sphere of Pt(II) (Table 1) shows that, after chloroquine coordination (complexes **5–8**), the electron density on the metal center decreased, as well as on the P atoms in the *trans* position of the Cl atom ( $\text{P}_{\text{a}}$ ), and at the same time the  $\text{P}_{\text{b}}$  (*trans* to  $\text{N}_1$ ) and  $\text{N}_1$  atoms were shielded. The phosphines and quinoline ligands bind to the metal atom through a combination of  $\sigma$ -donor ( $\text{L} \rightarrow \text{M}$ ) and  $\pi$ -acceptor ( $\text{L} \leftarrow \text{M}$ ) modes. When the  $\text{P}_{\text{b}}$  and chloroquine are mutually in the *trans* position to each other, they compete for the electron density residing in the d-orbital of the metal, and the predominating  $\pi$ -acceptor character of the ligands increases the electron density on the ligands, reducing their vulnerability to the magnetic field in NMR experiments. The deficient electron density on the platinum metal center is partially compensated by the other P atom ( $\text{P}_{\text{a}}$ ) and the chlorido ligand ( $\sigma$  and  $\pi$ -donor), leading to deshielding of the P atom and increasing its chemical shift toward the left side of the spectrum.

The ESI(+)-MS and ESI(+)-MS-MS spectra for the chloroquine platinum complexes (Figures S12–S17 in the Supporting Information) displayed, respectively, a signal corresponding to protonated molecule  $[\text{M}+\text{H}]^+$  and its fragmentations generating the product ions corresponding of the loss of hexafluorophosphate ion  $[\text{M}-\text{PF}_6]^+$ , followed by the loss of the chloroquine ligand  $[\text{M}-\text{PF}_6-\text{CQ}]^+$  and a peak corresponding to the free ligand  $[\text{CQ}+\text{H}]^+$ .

The Pt(II)/chloroquine complexes were studied by cyclic voltammetry experiments in acetonitrile solutions, and the data are given in the Supporting Information. In the cyclic voltammograms of complexes **5–8** (Figure S18 in the

Supporting Information), an oxidation wave was shown with potential values in the range of 1860–1943 mV (**I**) corresponding to the oxidation of  $\text{Pt}^{\text{II}} \rightarrow \text{Pt}^{\text{III}}$ . In addition, all the complexes exhibited other irreversible oxidation waves in the range of 870–900 mV (**II**), corresponding to oxidation of the amino-alkyl chain of chloroquine.<sup>28,29</sup> Finally, it was observed that complex **8** displayed a reversible process with  $E_{1/2} = 1048$  mV (**III/IV**) referent to ferrocene ( $\text{Fe}^{\text{II}} \rightarrow \text{Fe}^{\text{III}}$ ) present in the phosphine ligand.<sup>30</sup>

**Interactions with DNA.** The landmark success of platinum complexes as anticancer drugs is directly linked to their strong interaction with DNA. The molecular design of our platinum complexes incorporates CQ, a known DNA intercalator, in the coordination sphere of the metal, in order to try to achieve a synergistic effect on antitumor activity. There are several physical chemical techniques that can supply information on the interaction of metal complexes with DNA.<sup>31</sup> For this, absorption titration of platinum complexes **5–8** with calf thymus (CT) DNA was performed by monitoring the perturbation of the absorption electronic spectrum of the platinum complex, after the addition of DNA, in order to determine the binding constant ( $K_b$ ). The absorption plots show that, by adding DNA to the solutions of each platinum complex until saturation, hypochromism of the absorbance maxima (346–350 nm), bathochromism of 2 nm, and three isosbestic points at 293, 310, and 372 nm appeared in the spectra (the latter was the only observed in complexes **5** and **8**). The absorption titration of complex **6** is shown in Figure 5, as an example (for the other compounds, see Figure S19 in the Supporting Information).

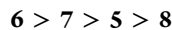
The corresponding binding constants ( $K_b$ ) and percent hypochromism ( $\Delta\epsilon$ ) for all the complexes are shown in Table 2. Generally, hypochromism and a red shift are associated with the interaction of the complex to the DNA helix, the binding constants calculated using a Scatchard equation show the following trends:

**Table 2.** Binding Constants for the Interaction between Pt(II) Complexes (5–8) and Calf Thymus (CT) DNA

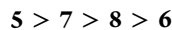
| complex           | $\Delta\epsilon$ (%) | $\lambda$ (nm) | $K_{b1}$ ( $\times 10^6 \text{ M}^{-1}$ ) | $K_{b2}$ ( $\times 10^5 \text{ M}^{-1}$ ) |
|-------------------|----------------------|----------------|---|---|
| 5                 | $41.33 \pm 4.18$     | 350            | $2.28 \pm 0.49$                           | $1.76 \pm 0.32$                           |
| 6                 | $18.54 \pm 0.78$     | 348            | $3.10 \pm 0.66$                           | $1.32 \pm 0.22$                           |
| 7                 | $13.94 \pm 1.37$     | 348            | $2.53 \pm 0.12$                           | $1.74 \pm 0.11$                           |
| 8                 | $34.37 \pm 1.32$     | 350            | $1.74 \pm 0.34$                           | $1.53 \pm 0.51$                           |
| CQ <sup>a</sup>   | $8.43 \pm 1.11$      | 346            | $1.44 \pm 0.33$                           | $1.28 \pm 0.10$                           |
| CQDP <sup>b</sup> | $15.18 \pm 3.74$     | 346            | $1.52 \pm 0.35$                           | $1.47 \pm 0.56$                           |

<sup>a</sup>CQ = chloroquine. <sup>b</sup>CQDP = chloroquine diphosphate.

for  $K_{b1}$ :



for  $K_{b2}$ :



These values are similar to those obtained for other platinum chloroquine compounds<sup>32</sup> and other metal complexes.<sup>33,34</sup> This indicates that these platinum chloroquine complexes interact with DNA more strongly than free CQ and CQDP, under the same conditions.

Viscosity is very sensitive to changes in the length of the DNA double helix, and it is considered to be one of the most unambiguous methods to determine the intercalation or nonintercalation binding modes of complexes to DNA in solution.<sup>6</sup> The effect of increasing amounts of complexes on the relative viscosities of CT-DNA is shown in Figure 6, together with other drugs (CQDP and cisplatin (CDDP)), for comparison purposes. The relative viscosity of CT-DNA was increased in the presence of CQDP and CQ, because of the lengthening of its double helix, as a result of the intercalation of these molecules with DNA base pairs. This behavior is also presented by the complex  $[\text{Ru}(\text{bpy})_2(\text{dppz})]^{2+}$ , the behavior of which is similar to that of the classic intercalator, ethidium bromide.<sup>35</sup> The results of viscosity measurements of platinum complexes 5–8 showed a marked decrease in the relative viscosity of CT-DNA (mainly 6 and 7) with an increase in the [complex]/[DNA] ratio, modifying the behavior exhibited by the free CQ. This decrease in the DNA viscosity can be attributed to a strong interaction between the platinum metal center and CT-DNA, thus decreasing the volume of the

biomolecule's structure, similar to the behavior shown by cisplatin (CDDP), which is known to exhibit strong interactions with DNA. The result suggests that the platinum/CQ complexes are nonintercalators, and that their behavior is governed mainly by the metal center, and not by the coordinated CQ.

The circular dichroism (CD) technique is very sensitive for diagnosing changes in the secondary structure of DNA resulting from DNA interactions with small molecules.<sup>36,37</sup> A typical CD spectrum of CT DNA shows a maximum at 275 nm, because of the base stacking, and a minimum at 248 nm, which is attributed to the right-handed helicity of the molecule, characteristic of its B conformation. Figure 7 shows the spectra of all four complexes evaluated with CT DNA solutions at different ratios, as well as the CD spectrum of DNA alone. All the complexes (5–8) produced significant changes in the ellipticity values for both bands, indicating that they modify the DNA secondary structure, as already reported for cisplatin and other platinum complexes.<sup>38</sup> These changes were more pronounced for complexes 6 and 7, which showed major changes in the viscosity studies. These modifications could be attributable to covalent binding of the complexes with DNA.<sup>39</sup>

The DNA plasmid has two main forms: the native state supercoiled (SC) and the open circular (OC) forms, but it sometimes also presents the linear form (L). Changes in electrophoretic mobility of any form are usually taken as evidence of direct metal–DNA interactions.<sup>31</sup> The modifications to the tertiary structure of the DNA plasmid pBR322 was studied by electrophoresis. CQ did not cause any significant effect on the mobility of the SC, OC, or L forms (see Figure S20 in the Supporting Information), indicating that this drug does not induce a noticeable alteration in the tertiary structure of the plasmid under these conditions. In the case of compounds 5–8, when the complex/DNA ratio increased, no bands are visible for DNA, either relaxed or linear due to the fragmentation of the duplex helix to DNA, as already reported.<sup>40</sup> This study suggest that compounds 5–8 have stronger interactions with the plasmid DNA than the cisplatin under the same experimental conditions.<sup>41</sup> Figure S20 shows that complexes 6 and 7 had stronger interactions than 5 and 8 (8 > 5), as has been shown in previous DNA interaction studies involving these complexes.

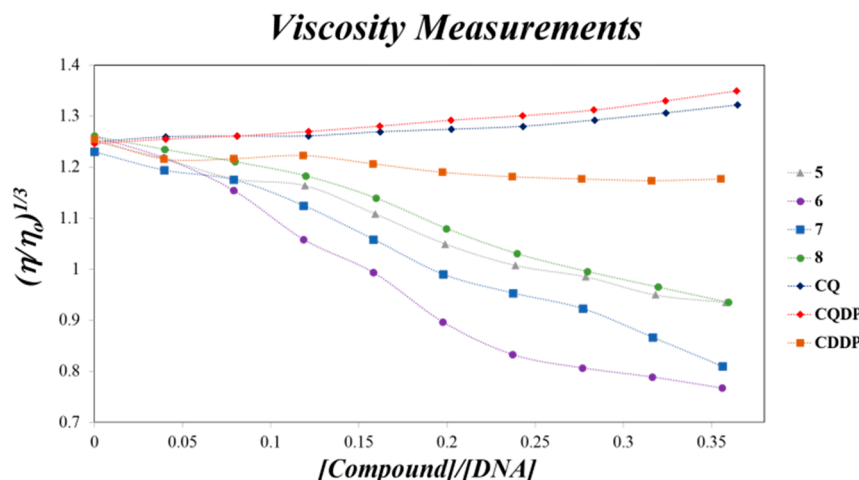


**Figure 6.** Effect of increasing concentration of Pt(II)/phosphine–chloroquine complexes and other drugs on the relative viscosity of CT-DNA at 25 °C.

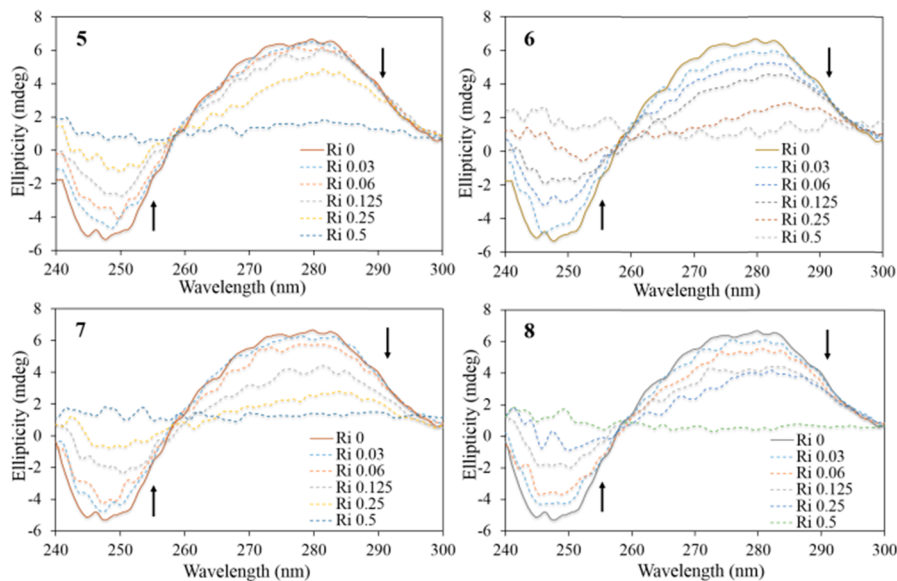


**Figure 7.** Circular dichroism (CD) spectra of CT DNA incubated 18 h with the complexes **5–8** at different [complex]/[DNA] ratios at 37 °C.

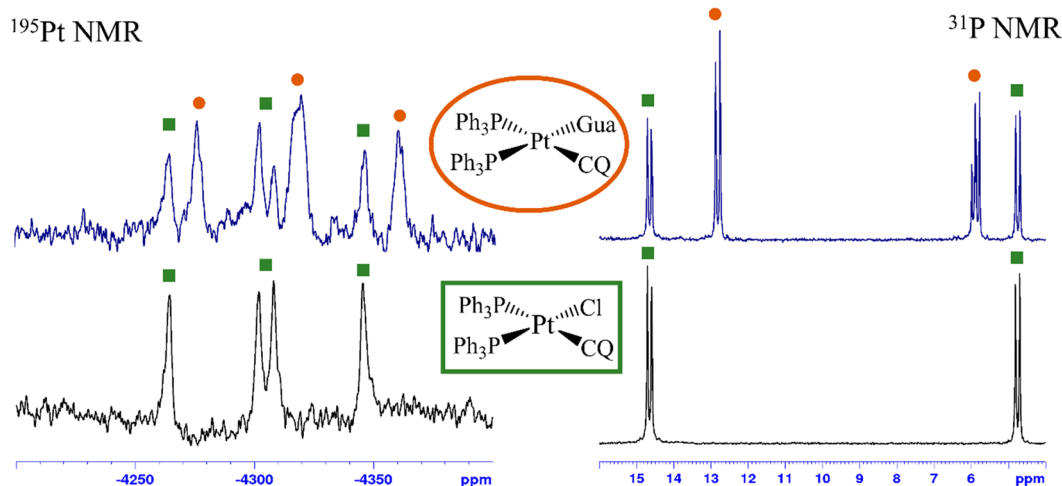


**Figure 8.**  $^{195}\text{Pt}\{^1\text{H}\}$  and  $^{31}\text{P}\{^1\text{H}\}$  NMR spectrum in DMSO for complex **5** (lower spectrum) and the mixture of **5** and an excess of guanosine (1:1.2) immediately after sample preparation (upper spectrum); where the signals corresponding to complex **5** (denoted by green squares) and complex **5**-guanosine (denoted by orange circles) are shown.

A summary of all studies of interaction of complexes **5–8** with the DNA suggests that these interactions are dominated by the covalent characteristics of the platinum metal center and not by the chloroquine ligand itself.

**Reaction between Complex 5 and Guanosine.** Platinum-based drugs can be activated by the dissociation of one chlorido and binding readily to DNA and other nucleophiles.<sup>42</sup> For this reason, the reaction between complex **5** and guanosine was studied, to check the possible lability of the chlorido ligand present in the complex. Figure 8 show the  $^{195}\text{Pt}\{^1\text{H}\}$  and  $^{31}\text{P}\{^1\text{H}\}$  NMR spectrum for complex **5** and the mixture of complex **5** and guanosine, immediately after the mixture of the reagents, observing the decrease of the signal for complex **5** (green square) and the surging of the new signals group corresponding to complex **5**-guanosine (orange circle). Figure S21B in the Supporting Information provides the  $^1\text{H}$  NMR spectrum of the mixture of complex **5** and guanosine (1:1.2), where the signals corresponding to free ( $X_f$ ) and bound ( $X_b$ ) guanosine are indicated. In this case, all the guanosine

signals suffer modifications in chemical shift, mainly NH, H8, NH<sub>2</sub>, and H1' (0.69, 0.06, 0.34, and 0.20 ppm, respectively); NH and NH<sub>2</sub> had the greatest variation, which may have been generated by intermolecular and/or intramolecular hydrogen bonds. The other signals reveal that the imidazole region of guanosine suffered greater disturbances after binding to the metal center, suggesting the coordination of guanosine to platinum through N7, as reported in the literature for similar platinum(II) complexes.<sup>43</sup>

**Interactions with BSA.** It has been found that the interaction of drugs with blood plasma proteins is a very important property, particularly regarding serum albumin, and is directly involved in the transport of drugs through the bloodstream. Usually, the binding of drugs to these plasma proteins may lead to either a loss or enhancement of the biological properties of the original drug.<sup>44</sup> To understand the mechanism of interaction between the complexes **5–8** and BSA, fluorescence quenching experiments were performed. The fluorescence properties of BSA arise from the intrinsic

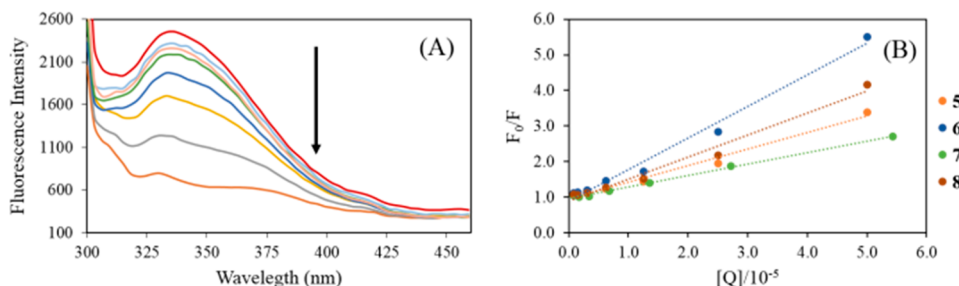


**Figure 9.** (A) Fluorescence quenching spectra of BSA with different concentrations of complex 7 with the excitation wavelength at 280 nm, at 310 K in a Trizma buffer, pH 7.4. The arrow shows the intensity changes upon increasing the concentration of the quencher. (B) Stern–Volmer plots showing tryptophan quenching in BSA at 310 K.

**Table 3. Stern–Volmer Quenching Constant ( $K_{sv}$ ), Biomolecular Quenching Rate Constant ( $K_q$ ), Biomolecular Binding Constant ( $K_b$ ), Number of Binding Sites ( $n$ ),  $\Delta G^0$ ,  $\Delta H^0$ , and  $\Delta S^0$  Values for Complex-BSA Systems at Different Temperatures**

| temperature (K)  | $K_b$ ( $\times 10^5 \text{ M}^{-1}$ ) | $K_{sv}$ ( $\times 10^4 \text{ M}^{-1}$ ) | $K_q$ ( $\times 10^{12} \text{ M}^{-1}$ ) | $n$             | $\Delta G$ (kJ mol $^{-1}$ ) | $\Delta H$ (kJ mol $^{-1}$ ) | $\Delta S$ (J mol $^{-1}$ K) |
|------------------|--|---|---|-----------------|------------------------------|------------------------------|------------------------------|
| <b>Complex 5</b> |  |   |   |                 |                              |                              |                              |
| 295              | $0.53 \pm 0.01$                        | $4.68 \pm 0.35$                           | $7.55 \pm 0.57$                           | $1.01 \pm 0.11$ | -26.39                       |                              |                              |
| 300              | $0.73 \pm 0.01$                        | $4.77 \pm 0.36$                           | $7.69 \pm 0.58$                           | $1.03 \pm 0.11$ | -26.92                       |                              |                              |
| 305              | $1.52 \pm 0.01$                        | $4.84 \pm 0.37$                           | $7.80 \pm 0.59$                           | $1.10 \pm 0.07$ | -27.37                       | 2.43                         | 97.65                        |
| 310              | $1.77 \pm 0.01$                        | $4.91 \pm 0.33$                           | $7.91 \pm 0.54$                           | $1.12 \pm 0.06$ | -27.85                       |                              |                              |
| <b>Complex 6</b> |  |   |   |                 |                              |                              |                              |
| 295              | $13.26 \pm 0.01$                       | $5.59 \pm 0.25$                           | $9.02 \pm 0.41$                           | $1.25 \pm 0.06$ | -26.82                       |                              |                              |
| 300              | $17.98 \pm 0.01$                       | $6.01 \pm 0.28$                           | $9.69 \pm 0.45$                           | $1.28 \pm 0.07$ | -27.49                       | 8.62                         | 120.10                       |
| 305              | $27.86 \pm 0.01$                       | $6.26 \pm 0.38$                           | $10.10 \pm 0.63$                          | $1.31 \pm 0.07$ | -28.03                       |                              |                              |
| 310              | $30.83 \pm 0.01$                       | $6.65 \pm 0.39$                           | $10.72 \pm 0.63$                          | $1.32 \pm 0.06$ | -28.63                       |                              |                              |
| <b>Complex 7</b> |  |   |   |                 |                              |                              |                              |
| 295              | $1.94 \pm 0.01$                        | $2.54 \pm 0.04$                           | $4.09 \pm 0.06$                           | $1.20 \pm 0.09$ | -24.90                       |                              |                              |
| 300              | $10.29 \pm 0.01$                       | $2.79 \pm 0.03$                           | $4.49 \pm 0.05$                           | $1.35 \pm 0.15$ | -25.54                       | 11.59                        | 123.64                       |
| 305              | $15.79 \pm 0.01$                       | $2.97 \pm 0.03$                           | $4.78 \pm 0.05$                           | $1.39 \pm 0.10$ | -26.14                       |                              |                              |
| 310              | $16.96 \pm 0.01$                       | $3.20 \pm 0.03$                           | $5.16 \pm 0.06$                           | $1.39 \pm 0.11$ | -26.75                       |                              |                              |
| <b>Complex 8</b> |  |   |   |                 |                              |                              |                              |
| 295              | $1.48 \pm 0.01$                        | $5.62 \pm 0.36$                           | $9.06 \pm 0.58$                           | $1.09 \pm 0.03$ | -26.84                       |                              |                              |
| 300              | $1.99 \pm 0.01$                        | $5.80 \pm 0.32$                           | $9.35 \pm 0.51$                           | $1.12 \pm 0.04$ | -27.41                       | 4.75                         | 107.01                       |
| 305              | $2.92 \pm 0.01$                        | $5.98 \pm 0.34$                           | $9.64 \pm 0.55$                           | $1.15 \pm 0.04$ | -27.91                       |                              |                              |
| 310              | $4.05 \pm 0.01$                        | $6.17 \pm 0.27$                           | $9.85 \pm 0.45$                           | $1.18 \pm 0.03$ | -28.44                       |                              |                              |

characteristics of the proteins, mainly due to the presence of tryptophan and tyrosine residues. Alterations in the emission spectra of BSA arise primarily from its tryptophan residues, because of protein conformational changes, subunit association, substrate binding, or denaturation. Quenching can occur by different mechanisms, usually classified as dynamic or static quenching, which can be distinguished one from the other by their variable dependence on temperature and viscosity, or preferably by lifetime measurements.<sup>45</sup> Figure 9A shows the modifications to the fluorescence electronic spectrum of BSA when the platinum complex concentration was increased.

In order to ascertain the fluorescence quenching mechanism, experiments were performed at different temperatures (295, 300, 305, and 310 K). As the temperature increased, a rise in the Stern–Volmer quenching constant ( $K_{sv}$ ) values was observed for all complexes, indicative of a dynamic mechanism. On the other hand, the biomolecular quenching rate constant ( $K_q$ ) values were above  $2.0 \times 10^{10} \text{ M}^{-1} \text{ s}^{-1}$ , which is the maximum possible value for dynamic quenching;<sup>46</sup> this is characteristic of static mechanisms, suggesting the presence of both mechanisms in the interaction of platinum complexes 5–8 with BSA. The binding constant ( $K_b$ ) and the number of binding sites ( $n$ ) were calculated from the slopes of the static quenching equation:  $\log(F_o - F)/F \text{ vs } \log[Q]$  (see Figure S22)

in the Supporting Information. The values of  $n$  (1.01–1.39) were approximately equal to 1, indicating that (i) the binding site in BSA is unique and (ii) the hydrophobic environment of the tryptophan residue is easily accessible by the complexes.<sup>47</sup> The binding constants obtained were ranked as

$$\mathbf{6} > \mathbf{7} \gg \mathbf{8} > \mathbf{5}$$

which is very similar to that found for  $K_{b1}$  in the DNA titrations; note that the values of complexes 6 and 7 are consistently 1 order of magnitude higher than those presented by complexes 5 and 8, indicating that the complexes that showed stronger interactions with DNA also presented higher affinities for BSA.

Finally, to identify the type of interaction between complexes and BSA, which include hydrophobic forces of interaction, electrostatic interactions, van der Waals interactions, and hydrogen bonds, the thermodynamic parameters were determined, including free-energy changes ( $\Delta G$ ), enthalpy changes ( $\Delta H$ ), and entropy changes ( $\Delta S$ ). The first shows the spontaneity of the reaction (or lack thereof), while the combination of the signs of the second and third parameters indicate the type of interaction. When  $\Delta H$  and  $\Delta S$  are positive, this corresponds to the involvement of hydrophobic forces in protein binding, while negative values of  $\Delta H$  and  $\Delta S$

**Table 4.** *In Vitro* Cytotoxicity of Complexes 5–8, CQ, and CDDP against MDA-MB-231, MCF-7, A549, DU-145 Tumor Cell Lines, and V79-4 (Chinese Hamster Lung Fibroblast Cells) and L929 (Nontumor Cell Line from Mice), after 48 h of Incubation<sup>a</sup>

|      | Cytotoxicity, IC <sub>50</sub> ( $\mu$ M) |               |              |              |              |              |
|------|---|---------------|--------------|--------------|--------------|--------------|
|      | MDA-MB-231                                | MCF-7         | A549         | DU-145       | V79-4        | L929         |
| 5    | 5.51 ± 0.30                               | 9.88 ± 0.63   | 6.81 ± 1.05  | 5.50 ± 0.83  | 1.26 ± 0.11  | 1.90 ± 0.44  |
| 6    | 28.04 ± 3.48                              | 7.52 ± 0.14   | 5.10 ± 0.08  | 49.61 ± 0.62 | 14.43 ± 1.65 | 21.09 ± 0.75 |
| 7    | 21.46 ± 3.50                              | 19.16 ± 1.10  | 8.13 ± 0.13  | 17.13 ± 2.92 | 12.18 ± 1.57 | 16.83 ± 2.43 |
| 8    | 6.37 ± 0.23                               | 9.27 ± 3.14   | 9.37 ± 0.56  | 29.36 ± 1.57 | 25.42 ± 2.41 | 5.02 ± 0.82  |
| CQ   | >200                                      | 82.01 ± 11.62 | 56.53 ± 9.18 | 79.50 ± 7.50 | 25.85 ± 2.95 | 25.94 ± 4.46 |
| CDDP | 2.44 ± 0.20                               | 13.98 ± 2.02  | 14.42 ± 1.45 | 2.33 ± 0.40  | 21.60 ± 1.28 | 16.53 ± 2.38 |

<sup>a</sup>Values are mean ± standard error from three independent experiments done in triplicate.

correspond to van der Waals and hydrogen bonding interactions; when  $\Delta H$  is negative and  $\Delta S$  is positive, this indicates electrostatic interactions.<sup>48</sup> The values (which are shown in Table 3) revealed that all four complexes showed the same behavior of spontaneous interaction with the protein, through hydrophobic forces.

**Cytotoxic Activity.** The platinum complexes were screened at different concentrations to determine their cytotoxicity against four human tumor cell lines and two nontumor cell lines, using the MTT assay.<sup>49</sup> The results obtained using this assay are listed in Table 4. Before performing the biological screening, the stability of the complexes was tested using the <sup>31</sup>P{<sup>1</sup>H} NMR technique in Tris-HCl solution containing 30% dimethylsulfoxide (DMSO). After 48 h, the spectra of the complexes were the same when compared with those recorded using fresh solutions. Comparing the cytotoxicities elicited by free CQ and the corresponding platinum complexes 5–8, it was observed that the metal complexes showed cytostatic effects at appreciably lower doses, under the same conditions, for all cell lines. Moreover, wide variation was observed in the evaluated IC<sub>50</sub> values (1–10  $\mu$ M for 5, 5–50  $\mu$ M for 6, 8–22  $\mu$ M for 7; and 5–29  $\mu$ M for 8). It was noted that complex 5 displayed the lowest IC<sub>50</sub> value (1–10  $\mu$ M), indicating its high potential as an antitumor drug, while 6 exhibited the lowest anticancer potential against DU-145 cells, although it showed selectivity for the MCF-7 and A549 tumor cell lines. Based on these results, the antitumor potential of the complexes can be arranged in the order



Changes in cell shape can be observed under an inverted microscope. The MDA-MB-231 breast cancer cells in the control group presented a spindle-shaped phenotype and there were very few round cells. The platinum complexes did not alter MDA-MB-231 cell morphology, even after 24 h of incubation, compared with control cells (Figure 10); however, after 48 h of incubation, the morphology was profoundly altered in MDA-MB-231 cells, involving a loss of adhesion, modifications to the spindle-shaped form, decreased confluence, and reduced cell numbers. There were more round cells, when compared to the control cells, which is indicative of cell detachment, probably because of apoptotic cell death.

The clonogenic or colony formation assay is an *in vitro* cell survival assay based on the ability of a single cell to grow into a colony, which is defined to consist of at least 50 cells. This assay is a widely used method to study the number and size of tumor cell colonies that remain after cytotoxic agent administration and serves as a measure of the antiproliferative effect of these treatments.<sup>50</sup> The ability to inhibit colony formation was tested

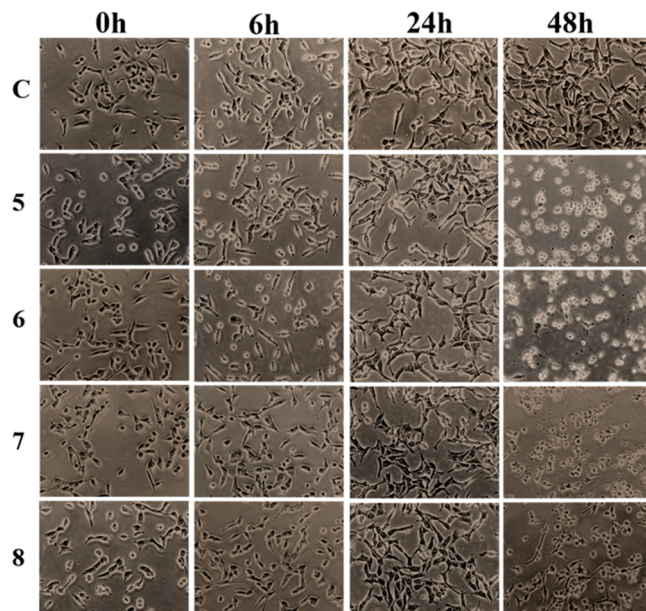


**Figure 10.** Cellular morphology of MDA-MB-231. Cells were allowed to grow in a humidified incubator at 37 °C in 5% CO<sub>2</sub> overnight and then treated with 5  $\mu$ M of complexes 5 and 8 or 15  $\mu$ M of complexes 6 and 7 for 48 h. Cell morphology was examined under an inverted microscope at 10 $\times$  magnification.

for complex 5 using MDA-MB-231 tumor cells (see Figure S24 in the Supporting Information). The complex decreased the colony number (Figure S24B) and size (Figure S24C) of MDA-MB-231 cells, compared with control cells, and this behavior was concentration-dependent (colony number, concentration: 141, 0.5  $\mu$ M; 133, 5  $\mu$ M; and 16, 15  $\mu$ M; colony size = 0.161–0.093 cm). The plating efficiency (PE) was calculated, and the results show that complex 5 significantly reduced the PE value at concentrations of 0.5  $\mu$ M (47%), 5  $\mu$ M (44%), and 15  $\mu$ M (5%), when compared to the PE of the control (53%) (see Figure S24D).

The ability of the tumor cells to migrate and invade the circulatory system and tissues is a key characteristic of metastasis. Therefore, the effects of platinum complexes on MDA-MB-231 tumor cell migration using wound assays was investigated (see Figure S25 in the Supporting Information). After 24 h incubation, the area covered by MDA-MB-231 cell migration was ~46% in control cells and ~38% in cells treated with 5, 6, and 7, whereas, for complex 8, the area covered was ~48%. Incubation for 48 h resulted in a clear inhibition of cell migration, compared with the migration of control cells. Complexes 5–8 markedly decreased the wound area closure of

MDA-MB-231 cells, while control cells repopulated 100% of the area after 48 h; complexes **5** and **6** only covered a wound area of ~42%, whereas **7** and **8** covered 49% and 59% of the wound area, respectively, in the same time period, and cell death was not observed. This supports the conclusion that complexes **5–8** inhibited the migration cells after 48 h of incubation, as observed in morphologic studies.

Finally, the biological activity of the phosphine chloroquine platinum(II) complexes was correlated with their interaction with the biological targets DNA and BSA. Thus, complexes **6** and **7** showed lower biological activities, even though they had greater interactions with DNA and the greatest affinities for BSA (an order of magnitude greater than **5** and **8**), indicating possible irreversible interactions with BSA, resulting in lower bioavailability to interact with DNA, thereby reducing their biological activity. However, at the same time, they are selective, suggesting that this family of compounds is promising for cancer drug development.

## CONCLUSIONS

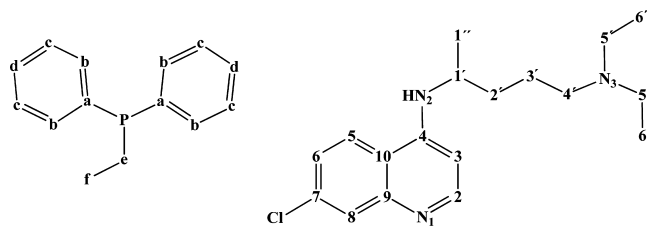
The synthesis and characterization of four chiral platinum(II) complexes featuring phosphine and chloroquine ligands were achieved, showing the atropisomeric phenomenon, which occurs both in solution and in the solid state. It was demonstrated that (i) the phosphine-Pt-CQ complexes *cis*-[PtCl(CQ)(PPh<sub>3</sub>)<sub>2</sub>]PF<sub>6</sub> (**5**), [PtCl(CQ)(dppp)]PF<sub>6</sub> (**6**), [PtCl(CQ)(dppb)]PF<sub>6</sub> (**7**), and [PtCl(CQ)(dpfp)]PF<sub>6</sub> (**8**) had high affinity by BSA and interacted with DNA more strongly than chloroquine and CQDP, and (ii) these interactions were dominated by the covalent characteristics of the platinum metal center and not by the chloroquine ligand. These results show that this family of Pt(II)/chloroquine compounds can be classified into two subgroups that are directly related to their structural similarities: the first set corresponds to complexes **5** and **8**, where two phenyl groups from the triphenylphosphine ligands are in the *cis* position presenting a  $\pi$ -stacking interaction, generating a very similar structure to that presented by the ligand dpfp; the second set corresponds to complexes **6** and **7**, where the difference of one CH<sub>2</sub> group in the alkyl chain of the biphosphine ligand did not seem to have a significant effect on the structure of the compounds.

The results of this study show a correlation between the ability of these complexes to interact with CT-DNA and BSA and their cytotoxic activity. Complex **5** showed the best cytotoxic profile on the four tumor cell lines (MDA-MB-231, MCF-7, A549, and DU-145) and, together with complex **8**, led to only minor modifications to the viscosity profiles and electrophoretic mobility of DNA. Complexes **5** and **8** also had lower affinity for BSA, considering the entire family of phosphine–chloroquine platinum(II) complexes studied here, which may lead to greater bioavailability. Complex **6** showed selectivity for tumor lines MCF-7 and A549. Based on these characteristics, [PtCl(CQ)(P)<sub>2</sub>]PF<sub>6</sub> complexes are promising anticancer drugs.

## EXPERIMENTAL SECTION

The characterization of the compounds under discussion are presented in the *Supporting Information*, along with crystallographic details and specifications of the materials for synthesis and instruments used for physical measurements.

**NMR Assignments.** The numbering schemes used for the assignment of the H, C, and N atoms present in the platinum(II) compounds **1–8** are shown.



**Synthesis of Complexes [PtCl<sub>2</sub>(P)<sub>2</sub>] (1–4).** The precursors were synthesized by modifying a previously reported method.<sup>51</sup> A solution of diphosphine (1.85 mmol or, in the case of PPh<sub>3</sub>, 3.70 mmol) in 60 mL of methanol and 80 mL of dichloromethane, in a Schlenk flask, was stirred until dissolution was complete. The K<sub>2</sub>[PtCl<sub>4</sub>] (1.81 mmol) and 15 mL of distilled water (biphasic system) were added to a flask that contained phosphine. The mixture was stirred and refluxed for 24 h, and the volume of the solvent was reduced under vacuum, obtaining a precipitate, which was filtrated, washed with hexane and diethyl ether, and dried under vacuum (for the experimental data, see the *Supporting Information*).

**Synthesis of Complexes [PtCl(CQ)(P)<sub>2</sub>]PF<sub>6</sub> (5–8).** In a Schlenk flask, a dichloromethane solution of [PtCl<sub>2</sub>(P)<sub>2</sub>] (0.78 mmol, 50 mL) was stirred until the dissolution of the solid was complete, and NH<sub>4</sub>PF<sub>6</sub> (0.51 g, 3.10 mmol) was added to the flask. CQ (0.46 g, 1.44 mmol) was dissolved in 40 mL of dichloromethane and also added to the mixture. The mixture was stirred and refluxed for 24 h, then the volume of the solvent was reduced under vacuum. The oil that formed was washed with water and diethyl ether and dried under vacuum (for the experimental data, see the *Supporting Information*).

**DNA Interaction Studies.** The absorption titrations were carried out by stepwise additions of a calf thymus (CT) DNA solution (1 mM, 5 mM Tris-HCl (pH 7.2), and 50 mM of NaCl buffer) to a solution of complexes **5–8** (70  $\mu$ M) in DMSO (20%), and the UV-vis spectra were recorded at 330 and 343 nm after each addition. The absorption of DNA was subtracted by adding the same amounts of CT DNA to the blank. The binding affinities were obtained using the Scatchard equation for ligand–macromolecule interactions with noncooperative binding sites:<sup>52,53</sup>

$$\frac{r}{C} = K(n - 1)$$

where *r* is the number of moles of platinum complexes bound to 1 mol of CT DNA (*C<sub>b</sub>*), *C<sub>DN</sub>A*), *n* the number of equivalent binding sites, and *K* the affinity of the complex for those sites. The concentrations of free complexes (*C<sub>f</sub>*) and bound complexes (*C<sub>b</sub>*) were calculated from the expressions

$$C_f = C(1 - \alpha)$$

and

$$C_b = C - C_f$$

where *C* is the total CQ-Pt concentration. The fraction of bound complex ( $\alpha$ ) was calculated according to

$$\alpha = \frac{A_f - A}{A_f - A_b}$$

where *A<sub>f</sub>* and *A<sub>b</sub>* are the absorbance of the free and fully bound platinum complexes at the selected wavelength, and *A* is the absorbance at any given point during the titration. *K<sub>b</sub>* is obtained from the slope of the plot.<sup>54</sup> The percent hypochromicity ( $\Delta\epsilon$ ) for compounds can be calculated using the equation

$$\Delta\epsilon (\%) = \frac{\epsilon_f - \epsilon_b}{\epsilon_f} \times 100$$

where  $\epsilon_b = A_b/C_b$ .

Viscosity measurements were carried out using an Ostwald viscometer that was immersed in a water bath maintained at 25 °C. DNA concentration (75 μM in 5 mM Tris–HCl (pH 7.2) plus 50 mM NaCl buffer) were kept constant in all samples, but the concentration of the compounds was increased from 0 μM to 75 μM. The flow time was measured at least five times with a digital stopwatch and the mean value was used. Data are presented as  $(\eta/\eta_0)^{1/3}$  versus the ratio [complex]/[DNA], where  $\eta$  and  $\eta_0$  are the specific viscosity of DNA in the presence and absence of the title complex, respectively. The values of  $\eta$  and  $\eta_0$  were calculated using the expression  $(t - t^b)/t^b$ , where  $t$  is the observed flow time and  $t^b$  is the flow time of the buffer alone. The relative viscosities of DNA were calculated as  $\eta/\eta_0$ .<sup>35</sup>

For the circular dichroism measurements, a solution of each complex was prepared in DMSO (1 mM). Appropriate volumes of this solution were added to 2 mL samples of a solution of CT DNA (100 μM) in Tris–HCl buffer (5 mM Tris–HCl, 50 mM NaCl, pH 7.2) to achieve molar ratios of 0–0.5 drug/DNA. The samples were incubated at 37 °C for 18 h. All CD spectra of DNA and of the DNA-drug adducts were recorded at 25 °C over the range of 240–640 nm and finally corrected with a blank and using noise reduction. The final data are expressed as molar ellipticity (in terms of millidegrees).<sup>38</sup>

For DNA electrophoresis assays, samples of 10 μL of the plasmid pBR322 (100 mM) were combined with the complex at different ratios and then incubated for 18 h at 37 °C. Five microliters of each sample were run (100 mV for 90 min) on a 1% agarose gel with TAE-1X (0.45 M Tris–HCl, 0.45 M acetic acid, 10 mM EDTA) and stained with ethidium bromide (2 μL ethidium bromide per 50 mL of the agarose gel mixture). The bands were then viewed, and the images were captured with ChemiDoc equipment.<sup>39</sup>

**BSA Interaction Studies.** Fluorescence spectroscopy is an effective method to explore the interactions between small molecules and biomacromolecules. The fluorescence of BSA comes from tryptophan, tyrosine, and phenylalanine residues, although the latter two amino acids contribute to fluorescence poorly.<sup>55</sup> The protein interaction was performed in 96-well plates for fluorescence assays. Bovine serum albumin ( $2.5 \times 10^{-6}$  M) was prepared by dissolving the protein in Tris–HCl and then dissolving the complexes in DMSO. For fluorescence measurements, the BSA concentration in Tris–HCl buffer was kept constant in all samples, while the complex concentration was increased from 0.78 μM to 100 μM. Quenching of the emission intensity of the tryptophan residues of BSA at 344 nm (excitation wavelength at 295 nm) was monitored at different temperatures (295, 300, 305, and 310 K). Experiments were carried out in triplicate and were analyzed using the classical Stern–Volmer equation:

$$\frac{F_0}{F} = 1 + K_q \tau_o [Q] = 1 + K_{sv} [Q] \quad (1)$$

where  $F_0$  and  $F$  are the fluorescence intensities in the absence and presence of the quencher, respectively;  $[Q]$  is the quencher concentration; and  $K_{sv}$  is the Stern–Volmer quenching constant, which can be written as

$$K_q = K_{sv} \tau_o$$

where  $K_q$  is the biomolecular quenching rate constant and  $\tau_o$  is the average lifetime of the fluorophore in the absence of the quencher ( $\tau_o = 6.2 \times 10^{-9}$  s).<sup>56</sup> Therefore, eq 1 was applied to determine  $K_{sv}$  by linear regression of a plot of  $F_0/F$  vs  $[Q]$ .

The binding constant ( $K_b$ ) and number of complexes bound to BSA ( $n$ ) were determined by plotting the double logarithmic graph of the fluorescence data using eq 2:

$$\log\left(\frac{F_0 - F}{F}\right) = \log K_b + n \log [Q] \quad (2)$$

The thermodynamic parameters were calculated from the van't Hoff equation:

$$\ln K = -\frac{\Delta H}{RT} + \frac{\Delta S}{R} \quad (3)$$

where the constant  $K$  is analogous to the Stern–Volmer quenching constant ( $K_{sv}$ ) at the corresponding temperature (295, 300, 305, and 310 K). Furthermore, the free-energy change ( $\Delta G$ ) was calculated using the conventional equation

$$\Delta G = -RT \ln K = \Delta H - T\Delta S \quad (4)$$

**Biological Experiments. Cell Lines and Culture.** *In vitro* cytotoxicity assays on cultured human tumor cell lines represent the standard method for the initial screening of antitumor agents. Thus, as a first step to assess their pharmacological properties, the platinum complexes were assayed using the human breast tumor cell lines MCF-7 (ATCC HTB-22) and MDA-MB-231 (ATCC HTB-26), the human prostate tumor cell line DU-145 (ATCC HTB-81), the human lung adenocarcinoma epithelial cell line A549 (ATCC CCL-185), the Chinese hamster lung fibroblast cell line V79-4 (ATCC CCL-93), and the L929 nontumor cell line from mice (ATCC CCL-1). The cells were routinely maintained in Dulbecco's Modified Eagle's medium (DMEM for L929, V79-4, MDA-MB-231, A549, and DU-145) or RPMI 1640 (for MCF-7) supplemented with 10% fetal bovine serum (FBS), L-glutamine (2 mM), penicillin (100 UI/mL), and streptomycin (100 mg/mL) at 37 °C in a humidified 5% CO<sub>2</sub> atmosphere.

**Cell Proliferation.** Briefly, all cell lines were prepared at a concentration of  $1.5 \times 10^4$  cells/150 μL, in complete medium (with 10% FBS), and plated on sterile 96 well plates for 24 h at 37 °C in a humidified 5% CO<sub>2</sub> atmosphere. The complexes were added to the wells in different concentrations and incubated for 48 h under the same conditions as described above. The cell proliferation assay was performed in comparison to the wells where the vehicle (0.5% DMSO) was added instead of the tested compounds. After incubation, the culture medium of each well was removed and a solution containing MTT (0.5 mg/mL) was added (100 μL/well). The plates were then kept at 37 °C for 4 h and the formed crystals were dissolved in isopropyl alcohol. The absorbance was read on an ELISA plate reader at a wavelength of 595 nm.

**Cell Morphology.** MDA-MB-231 and DU-145 growing cells were harvested, counted, and seeded at  $0.8 \times 10^5$  cells/well into 12-well plates. Cells were allowed to grow at 37 °C in a humidified 5% CO<sub>2</sub> atmosphere overnight and then, treated or not (control) with 2.5, 25, and 50 μM of 6 and 7 or 0.5, 5, and 25 μM of 5 and 8 for 0, 6, 24, and 48 h. Cell morphology was examined under an inverted microscope at 100× magnification.

**Colony Formation.** Growing MDA-MB-231 cells were harvested, counted, and seeded (300 cells) into petri dishes. Cells were allowed to grow at 37 °C in a humidified 5% CO<sub>2</sub> atmosphere overnight and then treated with different concentrations of complex 5 for 48 h. At this time point, the medium was changed to fresh medium without any compound. After incubation for an additional 10 days, the cells were rinsed with PBS, fixed with a solution 3:1 of methanol:acetic acid for 5 min and stained with 0.5% crystal violet for 25 min. Relative survival was calculated from the number of single cells that formed colonies of >50 cells on the 10th day. The plating efficiency (PE) was calculated as described in the work of Franken et al.<sup>50</sup>

$$PE = \frac{\text{number of colonies formed}}{\text{number of cells seeded}} \times 100$$

**Wound Healing.** MDA-MB-231 cells ( $1.0 \times 10^5$ /mL) were plated in 24-well plates and incubated until the culture reached 100% confluence. Afterward, a straight scratch was made with a sterile pipet tip and cells were washed with culture medium to remove unbound cells and debris. Cells were incubated with complexes 5–8 (lower values to IC<sub>50</sub>) for 24 and 48 h. The cells were visualized using an inverted microscope (Lake Success, NY, USA) at 40× total magnification and captured using a camera (Model XCST50, Sony, Park Ridge, NJ, USA) at 0, 24, and 48 h. The closure of the scratch area by migrating cells was measured using ImageJ software, and the percentage of scratch closure was calculated, comparing time zero and 48 h later, using the following formula:<sup>57</sup>

$$\text{wound closure (\%)} = \frac{A_{t=0h} - A_{t=\Delta h}}{A_{t=0h}} \times 100$$

## ■ ASSOCIATED CONTENT

### § Supporting Information

The Supporting Information is available free of charge on the ACS Publications website at DOI: [10.1021/acs.inorgchem.5b01647](https://doi.org/10.1021/acs.inorgchem.5b01647). Crystallographic data can be obtained free of charge from The Cambridge Crystallographic Data Centre via [www.ccdc.cam.ac.uk/data\\_request/cif](http://www.ccdc.cam.ac.uk/data_request/cif).

Supplementary crystallographic data ([ZIP](#))

Tables and figures providing the NMR and MS spectra of complexes 5–8 and X-ray crystallographic data of complex 7a ([PDF](#))

## ■ AUTHOR INFORMATION

### Corresponding Authors

\*E-mail: [wjvillarreal@gmail.com](mailto:wjvillarreal@gmail.com) (W. Villarreal).

\*E-mail: [daab@ufscar.br](mailto:daab@ufscar.br) (A. A. Batista).

### Notes

The authors declare no competing financial interest.

## ■ ACKNOWLEDGMENTS

The authors are grateful for the financial support provided by CNPq, CAPES and FAPESP (2013/02311-3).

## ■ REFERENCES

- (1) Rosenberg, B.; Van Camp, L.; Krigas, T. *Nature* **1965**, *205*, 698.
- (2) Varbanov, H.; Valiahdi, S.; Kowol, C.; Jakupc, M.; Galanski, M.; Keppler, B. *Dalton Trans.* **2012**, *41*, 14404.
- (3) Zhao, J.; Gou, S.; Sun, Y.; Fang, L.; Wang, Z. *Inorg. Chem.* **2012**, *51*, 10317.
- (4) Martínez, A.; Carreón, T.; Iniguez, E.; Anzellotti, A.; Sánchez, A.; Tyan, M.; Sattler, A.; Herrera, L.; Maldonado, R. A.; Sánchez-Delgado, R. A. *J. Med. Chem.* **2012**, *55*, 3867.
- (5) Barnes, K.; Kutikov, A.; Lippard, S. *Chem. Biol.* **2004**, *11*, 557.
- (6) Satyanarayana, S.; Dabrowiak, J. C.; Chaires, J. B. *Biochemistry* **1992**, *31*, 9319.
- (7) Tang, K.; Gan, H.; Li, Y.; Chi, L.; Sun, T.; Fuchs, H. *J. Am. Chem. Soc.* **2008**, *130*, 11284.
- (8) Barton, J. K. *Science* **1986**, *233*, 727.
- (9) Khan, N. H.; Pandya, N.; Prathap, K. J.; Kureshy, R. I.; Abdi, S. H. R.; Mishra, S.; Bajaj, H. C. *Spectrochim. Acta, Part A* **2011**, *81*, 199.
- (10) Sundquist, W. I.; Bancroft, D. P.; Lippard, S. J. *J. Am. Chem. Soc.* **1990**, *112*, 1590.
- (11) Park, G. Y.; Wilson, J. J.; Song, Y.; Lippard, S. J. *Proc. Natl. Acad. Sci. U. S. A.* **2012**, *109*, 11987.
- (12) Johnstone, T. C.; Lippard, S. J. *J. Am. Chem. Soc.* **2014**, *136*, 2126.
- (13) Sundquist, W. I.; Bancroft, D. P.; Chassot, L.; Lippard, S. J. *J. Am. Chem. Soc.* **1988**, *110*, 8559.
- (14) Valle, E. M.; do Nascimento, F. B.; Monteiro, M. C.; Machado, S.; Ellena, J.; Castellano, E. E.; Azevedo, E.; Ferreira, A. G.; Batista, A. A. *Quim. Nova* **2008**, *31*, 807.
- (15) Savarino, A.; Lucia, M. B.; Giordano, F.; Cauda, R. *Lancet Oncol.* **2006**, *7*, 792.
- (16) Jiang, P.-D.; Zhao, Y.-L.; Deng, X.-Q.; Mao, Y.-Q.; Shi, W.; Tang, Q.-Q.; Li, Z.-G.; Zheng, Y.-Z.; Yang, S.-Y.; Wei, Y.-Q. *Biomed. Pharmacother.* **2010**, *64*, 609.
- (17) O'Brien, R. L.; Allison, J. L.; Hahn, F. E. *Biochim. Biophys. Acta, Nucleic Acids Protein Synth.* **1966**, *129*, 622.
- (18) Meshnick, S. R. *Parasitol. Today* **1990**, *6*, 77.
- (19) Brown, J. M.; Perez-Torrente, J. J.; Alcock, N. W. *Organometallics* **1995**, *14* (3), 1195.
- (20) Bierbach, U.; Farrell, N. *JBIC, J. Biol. Inorg. Chem.* **1998**, *3*, 570.
- (21) Bierbach, U.; Farrell, N. *Inorg. Chem.* **1997**, *36*, 3657.
- (22) Brown, J. M.; Perez-Torrente, J. J.; Alcock, N. W.; Clase, H. J. *Organometallics* **1995**, *14* (1), 207.
- (23) Brissy, D.; Skander, M.; Retailleau, P.; Marinetti, A. *Organometallics* **2007**, *26* (24), 5782.
- (24) Ruiz, J.; Villa, M. D.; Cutillas, N.; López, G.; de Haro, C.; Bautista, D.; Moreno, V.; Valencia, L. *Inorg. Chem.* **2008**, *47* (11), 4490.
- (25) Tenorio, J. C.; Corrêa, R. S.; Batista, A. A.; Ellena, J. J. *Mol. Struct.* **2013**, *1048*, 274.
- (26) Navarro, M.; Vásquez, F.; Sánchez-Delgado, R. A.; Pérez, H.; Sinou, V.; Schrével, J. *J. Med. Chem.* **2004**, *47* (21), 5204.
- (27) Berners-Price, S.; Appleton, T. *Platinum-Based Drugs in Cancer Therapy*; Kelland, L., Farrell, N., Eds.; Springer Science Business Media: New York, 2000; p 22.
- (28) Mathur, N. C.; Goyal, R. N.; Malik, W. U. *Anal. Chim. Acta* **1990**, *230*, 91.
- (29) Radi, A. *Talanta* **2005**, *65*, 271.
- (30) Corain, B.; Longato, B.; Favero, G.; Ajò, D.; Pilloni, G.; Russo, U.; Kreissl, F. R. *Inorg. Chim. Acta* **1989**, *157*, 259.
- (31) Cutts, S. M.; Mastá, A.; Panousis, C.; Parsons, P. G.; Sturm, R. A.; Phillips, D. R. *Methods Mol. Biol.* **1997**, *90*, 95.
- (32) Navarro, M.; Castro, W.; Higuera-Padilla, A. R.; Sierraalta, A.; Abad, M. J.; Taylor, P.; Sánchez-Delgado, R. A. *J. Inorg. Biochem.* **2011**, *105*, 1684.
- (33) Navarro, M.; Castro, W.; Martínez, A.; Sánchez-Delgado, R. A. *J. Inorg. Biochem.* **2011**, *105*, 276.
- (34) Martínez, A.; Rajapakse, C. S. K.; Sánchez-Delgado, R. A.; Varela-Ramirez, A.; Lema, C.; Aguilera, R. J. *J. Inorg. Biochem.* **2010**, *104*, 967.
- (35) Haq, I.; Lincoln, P.; Suh, D.; Nordén, B.; Chowdhry, B. Z.; Chaires, J. B. *J. Am. Chem. Soc.* **1995**, *117*, 4788.
- (36) Ivanov, V. I.; Minchenkova, L. E.; Burckhardt, G.; Birch-Hirschfeld, E.; Fritzsche, H.; Zimmer, C. *Biophys. J.* **1996**, *71*, 3344.
- (37) Nordén, B.; Tjerneld, F. *Biopolymers* **1982**, *21*, 1713.
- (38) Macquet, J. P.; Butour, J. L. *Eur. J. Biochem.* **1978**, *83*, 375.
- (39) Zhang, B.; Seki, S.; Akiyama, K.; Tsutsui, K.; Li, T.; Nagao, K. *Acta Med. Okayama* **1992**, *46*, 427.
- (40) Sherman, S. E.; Lippard, S. J. *Chem. Rev.* **1987**, *87*, 1153.
- (41) Cohen, G. L.; Bauer, W. R.; Barton, J. K.; Lippard, S. J. *Science* **1979**, *203*, 1014.
- (42) Wang, D.; Lippard, S. J. *Nat. Rev. Drug Discovery* **2005**, *4*, 307.
- (43) Kozma, Á.; Ibáñez, S.; Silaghi-Dumitrescu, R.; Sanz Miguel, P.; Gupta, D.; Lippert, B. *Dalton Trans.* **2012**, *41*, 6094.
- (44) Ramachandran, E.; Raja, D. S.; Bhuvanesh, N. S.; Natarajan, K. *Dalton Trans.* **2012**, *41*, 13308.
- (45) Shang, L.; Wang, Y. Z.; Jiang, J. G.; Dong, S. J. *Langmuir* **2007**, *23*, 2714.
- (46) Zhao, X.; Liu, R.; Chi, Z.; Teng, Y.; Qin, P. *J. Phys. Chem. B* **2010**, *114*, 5625.
- (47) Gao, H.; Lei, L.; Liu, J.; Kong, Q.; Chen, X.; Hu, Z. *J. Photochem. Photobiol. A* **2004**, *167*, 213.
- (48) Ross, P.; Subramanian, S. *Biochemistry* **1981**, *20*, 3096.
- (49) Mosmann, T. *J. Immunol. Methods* **1983**, *65*, 55.
- (50) Franken, N.; Rodermond, H.; Stap, J.; Haveman, J.; Van Bree, C. *Nat. Protoc.* **2006**, *1*, 2315.
- (51) Dopeke, N.; Oemke, H. *Inorg. Chim. Acta* **2011**, *376*, 638.
- (52) McGhee, J. D.; Von Hippel, P. H. *J. Mol. Biol.* **1974**, *86*, 469.
- (53) Wei, C.; Jia, G.; Yuan, J.; Feng, Z.; Li, C. *Biochemistry* **2006**, *45*, 6681.
- (54) Cusumano, M.; Di Pietro, M. L.; Giannetto, A. *Inorg. Chem.* **1999**, *38*, 1754.
- (55) Carter, D. C.; Ho, J. X. *Adv. Protein Chem.* **1994**, *45*, 153.
- (56) Gratton, E.; Silva, N.; Mei, G.; Rosato, N.; Savini, I.; Finazzi-Agro, A. *Int. J. Quantum Chem.* **1992**, *42*, 1479.
- (57) Yue, P. Y.; Leung, E. P.; Mak, N. K.; Wong, R. N. *J. Biomol. Screening* **2010**, *15*, 427.